IEICE TRANSACTIONS

on Electronics

DOI:10.1587/transele.2024REP0001

Publicized:2024/09/06

This advance publication article will be replaced by the finalized version after proofreading.

A PUBLICATION OF THE ELECTRONICS SOCIETY

The Institute of Electronics, Information and Communication Engineers
Kikai-Shinko-Kaikan Bldg., 5-8, Shibakoen 3chome, Minato-ku, TOKYO, 105-0011 JAPAN

PAPER *Special Section on Recent Progress in Electromagnetic Theory and Its Application*

High Frequency Plane Wave Scattering Analysis by Large Buildings with Multiple Windows

Cuong Manh BUI[†a)], ***Student Member and*** **Hiroshi SHIRAI**[†b)], ***Fellow***

SUMMARY In this study, the scattering fields by multi-window buildings have been analyzed by using the Kirchhoff approximation method. The scattering fields are obtained by the radiation integrals due to the equivalent current sources excited by the incident plane wave on the exterior of the building and the virtually closed window apertures. The fields in the window region are represented by rectangular waveguide modes, then the reflected fields from window glasses are also converted to the equivalent currents. The validity of our formulation has been confirmed by numerical comparison with the physical optics method and by measurements on scale models. Discussions have been made on the impact of window glass in the context of high-frequency wireless communications.

key words: *Kirchhoff approximation, dielectric glass effect, multi-window building, building scattering.*

1. Introduction

In the field of wireless communications, researchers and developers are constantly improving their work to meet today's demands for device connectivity. Their efforts are not limited to increasing the quantity, but are also focused on enhancing the quality. Efforts have been made to develop innovative devices to prepare for an era marked by a vast number of devices connected at high speeds. The study focuses on the behavior of radio waves in urban environments.

It is a well-known fact that wall edges, windows, and glass panels of towering structures significantly affect radio wave propagation [1]. The effect of a window aperture on a building wall has been reported and analyzed by various methods [2]–[10]. The evaluation of the scattering by a building window can be considered similar to the problem of electromagnetic diffraction by an aperture perforated on an infinite perfectly conducting screen. The problem is reported and analyzed by many methods such as an eigenfunction expansion in Mathieu functions [2], the combination of Wiener-Hopf method and scattering matrix techniques [3], the combination of Fourier transform and mode-matching technique [4], [5], a hybrid method of finite element and boundary integral methods [6], [7], and the Kobayashi Potential method [8]–[10]. While the aforementioned studies provide valuable insights into the scattering by a single narrow aperture, it is important to note that these solutions could potentially be extended to scenarios involving multiple apertures. However, when the window size in real-world wireless communications is much larger than the wavelength, these methods may face numerical convergence issues.

Some high-frequency asymptotic methods, such as the Physical Optics (PO) [11]–[14], Geometrical Theory of Diffraction (GTD) [15]–[21], Ray Tracing (RT) [22], [23], or Kirchhoff Approximation (KA) [24]–[29] methods, may analyze the scattering field by large conducting objects. Generally, these asymptotic solutions should be applicable as long as $kl \gg 1$, where k is the wave number and l is a typical distance such as the building and window dimensions, while the accuracy may be low for a small kl [19]. The PO method may encounter difficulties in calculating the re-radiation field from the window aperture. While the GTD method might be applied only to the conducting objects, the RT method can be used to solve the scattering field of a building facade with multiple windows, each with dielectric glass. However, the RT method presents its own set of challenges: as the structure of the object becomes larger, there is a significant increase in the number of rays, which not only extends the calculation time but also demands high performance and considerable memory size. In previous studies [27]–[29], the KA method has been effectively applied to calculate the scattering fields for large windows apertures on an infinite screen. These studies have also investigated the importance and effects of vertical and horizontal polarizations. Based on these successful applications, this method is utilized to analyze the scattering fields by a building with multiple windows.

This research extends previous investigations that focused on the diffraction by a three-dimensional window containing a dielectric glass on an infinite conducting plate [29]. The current study expands this scope to consider an entire building with multiple windows. In the real-world scenario, buildings are situated on the ground, and the ground effect could influence the total scattering field. If one treats an isolated building on the ground, the ground effect may be estimated by the image theory. However, the impact of the high-rise building windows would be stronger than the effect of the height and the ground, as the building's foundation is usually obscured by other nearby small buildings and ground objects.

Utilizing the KA method, the scattering field by building structures can be interpreted as radiation from the magnetic currents distributed over both the virtually closed surfaces on the windows and the exterior surfaces of the building wall. By representing the electromagnetic field inside the window apertures in terms of rectangular waveguide modes,

[†]The authors are with the Graduate School of Science and Engineering, Chuo University, Tokyo, 112-8551, Japan
a) E-mail: a22.mfmp@g.chuo-u.ac.jp
b) E-mail: shirai@m.ieice.org

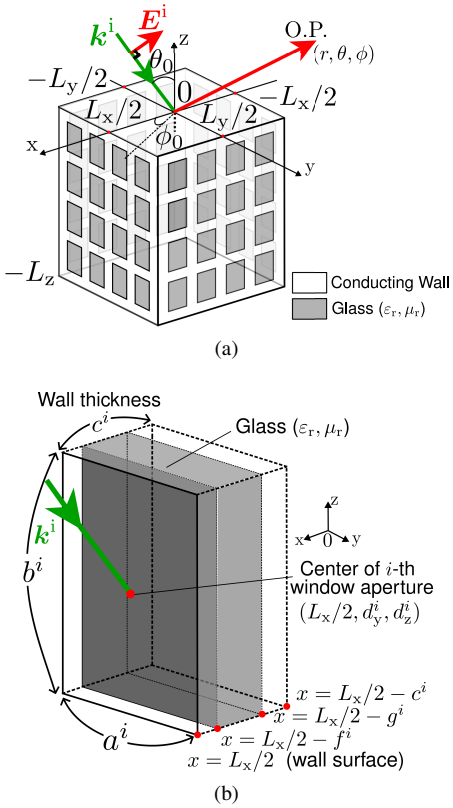

Fig. 1 Configuration of the problem. (a) A building with multiple glass windows. (b) i-th window on the side wall located at $x = L_{\mathrm{x}}/2$.

it is theoretically possible to calculate the reflection of the modal field at the window glass layer using waveguide modal theory, or only selected significant modes may be summed to express the field [24], [25].

The numerical results are computed and compared with the results obtained using the PO method in the commercial software Ansys HFSS and scale model measurements taken in an anechoic chamber room. Additional numerical results are provided to demonstrate the effect of window size and glass layer. For the subsequent discussion, it is assumed that the time-harmonic factor $e^{j\omega t}$ is omitted throughout the text.

2. Formulations

Figure 1 (a) describes a plane wave impinging on a roof of a building with dimensions $L_{\mathrm{x}}, L_{\mathrm{y}}, L_{\mathrm{z}}$. The building structure under consideration comprises four vertical walls with multiple glass windows and a horizontal roof. The vertical walls are situated at coordinates $x = \pm L_{\mathrm{x}}/2$ and $y = \pm L_{\mathrm{y}}/2$. Each conducting side wall has a thickness of c^i and contains N glass windows. Figure 1 (b) illustrates a detail of i-th window located on the vertical wall of the building at $x = L_{\mathrm{x}}/2$. The dimensions of this window are given by (a^i, b^i). The precise location of the window on the building's facade is given by $(d^i_{\mathrm{x}} = L_{\mathrm{x}}/2, d^i_{\mathrm{y}}, d^i_{\mathrm{z}})$. Inside the window, a window glass is simulated by a material slab layer whose relative material parameters are given by ε_{r} and μ_{r}, and the thickness is $g^i - f^i$. The location of the glass is determined by $L_{\mathrm{x}}/2 - f^i$.

An incident plane wave may be represented as

$$\boldsymbol{E}^{\mathrm{i}} = (A_\theta \hat{\boldsymbol{\theta}}_0 + A_\phi \hat{\boldsymbol{\phi}}_0) e^{-j\boldsymbol{k}^{\mathrm{i}} \cdot \boldsymbol{r}}. \tag{1}$$

where "^" denotes the corresponding unit vector, $\boldsymbol{k}^{\mathrm{i}}$, $\boldsymbol{r}$ represent the incident wave number vector, the position vector to the observation point (O.P.), respectively. At any given angle of the incident plane wave, at most only three surfaces of the building are illuminated. For practical situations, the communication signals propagate and are scattered almost horizontally ($\theta_0 \sim \theta \sim \pi/2$). In what follows, our present formulations are derived under the condition of the building being illuminated by a plane wave of horizontal polarization ($A_\theta = 0$, $A_\phi = 1$) and some numerical calculations have been done in the horizontal plane ($\theta_0 = \theta = \pi/2$). The scattering formulation for vertical polarization can be derived in a similar manner. While the corresponding scattering effects for the vertical polarization may also be as important as the one for the horizontal case, these are not included in this study due to page limitations.

According to the KA method, the scattering field may be given by the radiation from the equivalent magnetic currents induced on the exterior of the building and on the virtually closed window apertures as depicted in Fig. 2. The magnetic current sources $\boldsymbol{M}^{(1)}_{\pm}$, $\boldsymbol{M}^{(2)}_{\pm}$ excite the fields $\boldsymbol{E}^{(1)}_{\pm}$, $\boldsymbol{E}^{(2)}_{\pm}$ which represent the scattering fields by the outer edges. The scattering field $\overline{\boldsymbol{E}}^{(2)}$ by the windows is generated by the magnetic currents $\overline{\boldsymbol{M}}^{(2)}_{\pm}$ on the virtually closed apertures. The currents $\overline{\boldsymbol{M}}^{(2)}_{\pm}$ are a sum of currents generated by the original incident plane wave and the reflection field at the glass layer. The field inside each window may be expressed in terms of rectangular waveguide modes so that the reflection field at the material layer can be calculated theoretically by using waveguide modal theory. Detailed information about the field inside the window and its derivation can be found in Ref. [29]. If the windows are far apart and far from the wall edges, and these distances are bigger than the wavelength, then the interactions among them become insignificant and can be disregarded. Thus, the scattering field by the building can be calculated by combining the individual results for the building edges and windows. While there are scattered fields due to the conducting walls and window glasses, re-radiations from the internal field are not considered in the subsequent analysis.

2.1 Scattering fields by the outer edges of the building roof and side walls

Figure 2 (a) illustrates the magnetic currents on the exterior of the building. Equivalent currents $\boldsymbol{M}^{(1)}_{\pm}$ on the exterior of the building roof ($|x| > L_{\mathrm{x}}/2, |y| > L_{\mathrm{y}}/2, z = 0_{\pm}$) may be derived from the incident electric field as [24]

$$\boldsymbol{M}^{(1)}_{\pm}(x, y, z = 0_{\pm}) = \boldsymbol{E}^{\mathrm{i}}\Big|_{z=0_{\pm}} \times (\pm\hat{\boldsymbol{z}}). \tag{2}$$

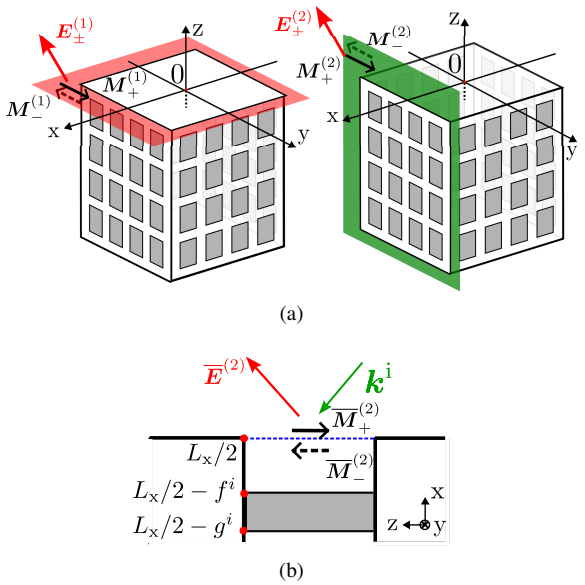

Fig. 2 Analysis of scattering fields created by magnetic currents. (a) Scattering fields created by magnetic currents on the exterior of the roof ($z = 0$) and side wall ($x = L_x/2$). (b) Scattering field excited by magnetic currents on i-th window aperture on the building side wall ($x = L_x/2$).

The far-field scattering field $\boldsymbol{E}_{\pm}^{(1)}$ may be derived as a radiation from the above equivalent magnetic sources $\boldsymbol{M}_{\pm}^{(1)}$ through a vector potential as [28]–[30],

$$\boldsymbol{E}_{\pm}^{(1)} = -\nabla\times\left[\frac{e^{-jkr}}{2\pi r}\int_{S'}\boldsymbol{M}_{\pm}^{(1)}(\boldsymbol{r}')e^{jk\boldsymbol{r}'\cdot\hat{\boldsymbol{r}}}dx'dy'\right], \tag{3}$$

where S' denotes the virtually closed exterior of the roof ($|x'| > L_x/2, |y'| > L_y/2, z' = 0$). $\boldsymbol{r}'$ is the position vector to the aperture source point on S'. When one executes the integral in Eq. (3), one should note that the result contains spurious reflected plane wave and missing incident plane wave due to the closed surface S' [19]. Accordingly, one may remove these geometrical optics fields to obtain the desired diffraction field*. By disregarding r^{-2} and higher-order terms, the scattering far-field expressions for $\boldsymbol{E}_{+}^{(1)}$ and $\boldsymbol{E}_{-}^{(1)}$ are combined and simplified into a unified form as follows

$$E_r^{(1)} \sim 0, \tag{4}$$

$$E_\theta^{(1)} \sim \mathrm{U}\left(\frac{\pi}{2}-\theta_0\right)\mathrm{sgn}\left(\frac{\pi}{2}-\theta\right)\frac{jA_\phi e^{-jkr}}{2\pi kr}k^2L_xL_y \cdot \mathrm{sinc}\left(\frac{\alpha kL_x}{2}\right)\mathrm{sinc}\left(\frac{\beta kL_y}{2}\right)\sin(\phi_0-\phi), \tag{5}$$

$$E_\phi^{(1)} \sim -\mathrm{U}\left(\frac{\pi}{2}-\theta_0\right)\mathrm{sgn}\left(\frac{\pi}{2}-\theta\right)\frac{jA_\phi e^{-jkr}}{2\pi kr}k^2L_xL_y \cdot \mathrm{sinc}\left(\frac{\alpha kL_x}{2}\right)\mathrm{sinc}\left(\frac{\beta kL_y}{2}\right)\cos\theta\cos(\phi_0-\phi), \tag{6}$$

where

$$\alpha = \sin\theta_0\cos\phi_0 + \sin\theta\cos\phi, \tag{7}$$

$$\beta = \sin\theta_0\sin\phi_0 + \sin\theta\sin\phi, \tag{8}$$

$$\gamma = \cos\theta_0 + \cos\theta, \tag{9}$$

and $\mathrm{U}(x)$, $\mathrm{sgn}(x)$ are unit step, sign functions, respectively.

The scattering far-field $\boldsymbol{E}_{\pm}^{(2)}$ by the building side wall at $x = L_x/2$ may be derived in the same manner as a radiation from equivalent magnetic current sources $\boldsymbol{M}_{\pm}^{(2)}$ ($\boldsymbol{M}_{+}^{(2)}$ on $x = L_x/2_+$, $\boldsymbol{M}_{-}^{(2)}$ on $x = L_x/2_-$). Then $\boldsymbol{E}_{\pm}^{(2)}$ may be combined as

$$E_r^{(2)} \sim E_\theta^{(2)} \sim 0, \tag{10}$$

$$E_\phi^{(2)} \sim \left[\mathrm{U}\left(\frac{\pi}{2}-\phi_0\right)+\mathrm{U}\left(\phi_0-\frac{3\pi}{2}\right)\right]\mathrm{sgn}\left(\phi-\frac{\pi}{2}\right)\mathrm{sgn}\left(\frac{3\pi}{2}-\phi\right) \cdot \frac{jA_\phi e^{-jkr}}{2\pi kr}k^2L_yL_ze^{-j\gamma kL_z/2}e^{j\alpha kL_x/2} \cdot \mathrm{sinc}\left(\frac{\gamma kL_z}{2}\right)\mathrm{sinc}\left(\frac{\beta kL_y}{2}\right)\sin\theta\cos\phi_0. \tag{11}$$

The scattered fields by other side walls can be formulated in a similar manner and these are given in the Appendix A.

2.2 Scattering fields by building windows

The evaluation of the scattering by a window may be estimated from the scattering by a hole perforated on a thick conducting screen. The fields inside the window can be expressed by rectangular waveguide modes. Based on the derivation of the scattering far-field by a window in Ref. [29] as well as the above assumption of no coupling among windows and building edges, the scattering field by N windows on the building wall at $x = L_x/2$ may be derived by the superposition of those by each window.

The modal reflection occurs when the rectangular waveguide modal fields are incident on the glass layer as in Fig. 2 (b). The reflection coefficients $R_{m,n}$ and $\overline{R}_{m,n}$ for TE_{mn}, TM_{mn} modes at the glass interface can be obtained as

$$R_{m,n} = \left[e^{2jk'_{m,n}(f^i-g^i)}-1\right]e^{-2jk_{m,n}f^i} \cdot \frac{(k'_{m,n})^2-(\mu_r k_{m,n})^2}{\left\{\begin{array}{l}(\mu_r k_{m,n}+k'_{m,n})^2 \\ \quad -(\mu_r k_{m,n}-k'_{m,n})^2e^{2jk'_{m,n}(f^i-g^i)}\end{array}\right\}}, \tag{12}$$

$$\overline{R}_{m,n} = \left[e^{2jk'_{m,n}(f^i-g^i)}-1\right]e^{-2jk_{m,n}f^i} \cdot \frac{(k'_{m,n})^2-(\varepsilon_r k_{m,n})^2}{\left\{\begin{array}{l}(\varepsilon_r k_{m,n}+k'_{m,n})^2 \\ \quad -(k'_{m,n}-\varepsilon_r k_{m,n})^2e^{2jk'_{m,n}(f^i-g^i)}\end{array}\right\}}, \tag{13}$$

with $k_{m,n}$, and $k'_{m,n}$ are the modal wave numbers outside and inside the glass layer as

$$k_{m,n} = k\sqrt{1-(m\pi/ka^i)^2-(n\pi/kb^i)^2}, \tag{14}$$

$$k'_{m,n} = k\sqrt{\varepsilon_r\mu_r-(m\pi/ka^i)^2-(n\pi/kb^i)^2}. \tag{15}$$

*These geometrical optics fields are not necessary for scattering far-field calculation.

The scattering field $\overline{\boldsymbol{E}}^{(2)}$ could be determined by summing the scattering contributions from each individual window as

$$\overline{E}_r^{(2)} \sim 0, \tag{16}$$

$$\begin{aligned}\overline{E}_\theta^{(2)} \sim & \left[\mathrm{U}\left(\frac{\pi}{2}-\phi_0\right)+\mathrm{U}\left(\phi_0-\frac{3\pi}{2}\right)\right]\left[\mathrm{U}\left(\frac{\pi}{2}-\phi\right)+\mathrm{U}\left(\phi-\frac{3\pi}{2}\right)\right] \\ & \cdot \frac{jA_\phi e^{-jkr}}{2\pi kr}\sum_{i=1}^{N} e^{jk[\alpha(L_x/2)+\beta d_y^i+\gamma d_z^i]} \\ & \cdot \sum_{m=0}^{\infty}\sum_{n=0}^{\infty}\frac{(k^2a^ib^i)^2B_{m,n}^{(2)}\cos\theta\cos\phi}{(m\pi/ka^i)^2+(n\pi/kb^i)^2} \\ & \cdot \left[\left(\frac{m\pi}{ka^i}\right)^2 R_{m,n}M_{m,n}^{(2)}+\frac{mn\pi^2}{k^2a^ib^i}\overline{R}_{m,n}N_{m,n}^{(2)}\right],\end{aligned} \tag{17}$$

$$\begin{aligned}\overline{E}_\phi^{(2)} \sim & \left[\mathrm{U}\left(\frac{\pi}{2}-\phi_0\right)+\mathrm{U}\left(\phi_0-\frac{3\pi}{2}\right)\right]\left[\mathrm{U}\left(\frac{\pi}{2}-\phi\right)+\mathrm{U}\left(\phi-\frac{3\pi}{2}\right)\right] \\ & \cdot \frac{jA_\phi e^{-jkr}}{2\pi kr}\sum_{i=1}^{N} e^{jk[\alpha(L_x/2)+\beta d_y^i+\gamma d_z^i]} \\ & \cdot \left\{k^2a^ib^i\,\mathrm{sinc}\left(\frac{ka^i\beta}{2}\right)\mathrm{sinc}\left(\frac{kb^i\gamma}{2}\right)\cos\phi_0\sin\theta\right. \\ & + \sum_{m=0}^{\infty}\sum_{n=0}^{\infty}\frac{(k^2a^ib^i)^2B_{m,n}^{(2)}\sin\phi}{(m\pi/ka^i)^2+(n\pi/kb^i)^2} \\ & \cdot \left\{R_{m,n}M_{m,n}^{(2)}\left[\left(\frac{n\pi}{kb^i}\right)^2\sin^2\theta-\left(\frac{m\pi}{ka^i}\right)^2\cos^2\theta\right]\right. \\ & \left.\left.-\frac{mn\pi^2}{k^2a^ib^i}\overline{R}_{m,n}N_{m,n}^{(2)}\right\}\right\},\end{aligned} \tag{18}$$

where

$$\begin{aligned}B_{m,n}^{(2)} = & \frac{(-1)^{m+1}e^{j(ka^i/2)\sin\theta\sin\phi}+e^{-j(ka^i/2)\sin\theta\sin\phi}}{(m\pi)^2-(ka^i\sin\theta\sin\phi)^2} \\ & \cdot \frac{(-1)^{n+1}e^{j(kb^i/2)\cos\theta}+e^{-j(kb^i/2)\cos\theta}}{(n\pi)^2-(kb^i\cos\theta)^2},\end{aligned} \tag{19}$$

$$M_{m,n}^{(2)} = -\frac{n^2\pi^2\epsilon_m\epsilon_n a^i}{2b^i}\sin\theta_0\sin(2\phi_0)\overline{B}_{m,n}^{(2)}, \tag{20}$$

$$N_{m,n}^{(2)} = -2mn\pi^2\sin\theta_0\sin(2\phi_0)\overline{B}_{m,n}^{(2)}, \tag{21}$$

$$\begin{aligned}\overline{B}_{m,n}^{(2)} = & \frac{(-1)^{m+1}e^{j(ka^i/2)\sin\theta_0\sin\phi_0}+e^{-j(ka^i/2)\sin\theta_0\sin\phi_0}}{(m\pi)^2-(ka^i\sin\theta_0\sin\phi_0)^2} \\ & \cdot \frac{(-1)^{n+1}e^{j(kb^i/2)\cos\theta_0}+e^{-j(kb^i/2)\cos\theta_0}}{(n\pi)^2-(kb^i\cos\theta_0)^2},\end{aligned} \tag{22}$$

and

$$\epsilon_j = \begin{cases}1 & (j=0)\\ 2 & (j>0).\end{cases} \tag{23}$$

In the present study, the derived KA formulas do not include a parameter to account for the wall thickness c^i. According to Ref. [29], the wall thickness c^i primarily does affect the scattering field inside the building, but not the outer field.

The scattering fields by windows of other side walls can be formulated similarly. These results are summarized in the Appendix A.

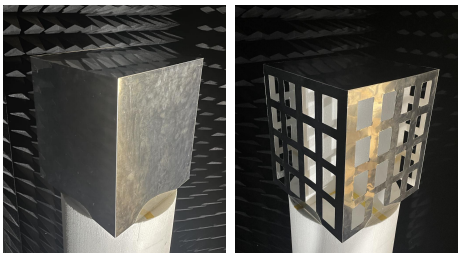

(a) No window model (b) 64 glassless windows model

Fig. 3 Building models for measurement. $L_x = L_y = 28$ cm, $L_z = 32$ cm. $a^i = 4$ cm, $b^i = 5.5$ cm. (a) No window model. (b) 64 glassless windows model.

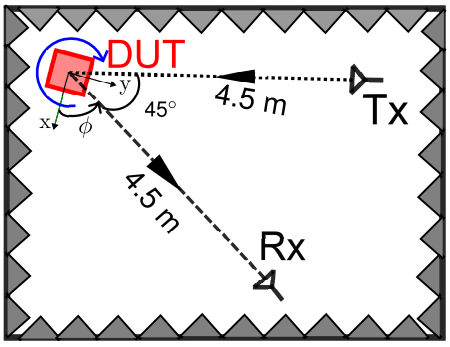

Fig. 4 Top view of the bistatic measurement setup in an anechoic chamber room.

3. Numerical Results and Discussion

In order to confirm the validity of our formulation, numerical calculations have been done for various parameters. While our formulation is valid for any set of window arrangements, as long as the distance between the window apertures is assumed to be electrically far. Some results are shown here for equally aligned window cases. In the subsequent numerical analysis, a common factor of $jA_\phi e^{-jkr}/(2\pi r)$ is used to normalize all far-field scattering patterns. For the calculation by window effects in Eqs. (17) and (18), infinite series of waveguide modes have been truncated with the propagating and the first three evanescent modes, but the multiple bouncing inside the window layer has been taken into account in the reflection coefficients in Eqs. (12) and (13) [27].

First, in order to evaluate the accuracy of our KA solution, two distinct models of a typical four-story building are constructed as shown in Fig. 3 for scale model measurements. Bistatic scattering measurements have been performed at 6.5 GHz in an anechoic chamber room as depicted in Fig. 4. Because of the tight chamber space, both the transmit (Tx) and receive (Rx) antennas are positioned 4.5 m away from the

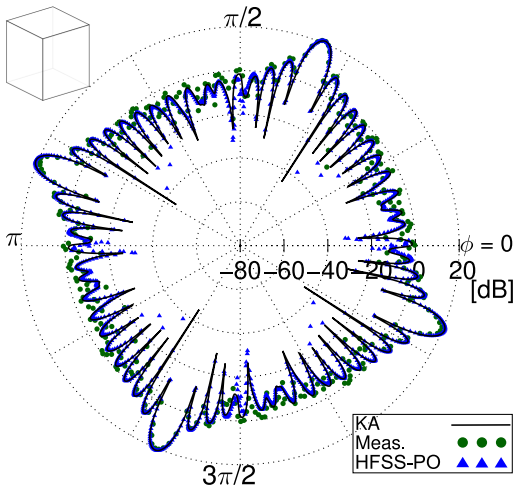

(a) No window

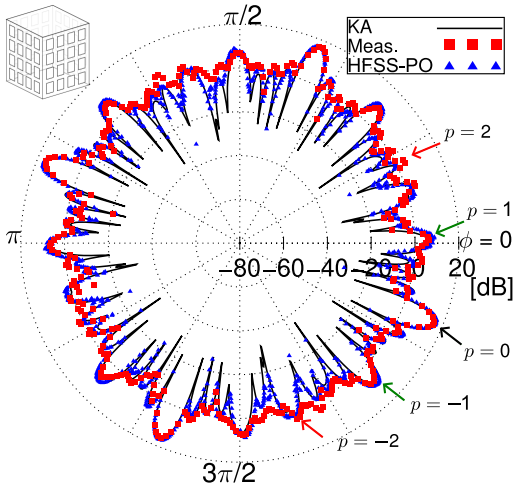

(b) 64 glassless windows

Fig. 5 Comparison of the bistatic scattering pattern E_ϕ between buildings with and without glassless windows. $f = 6.5$ GHz. $\theta_0 = \theta = \pi/2$. $\phi_0 = \phi + \pi/4$. $L_x = L_y = 6.09\lambda$, $L_z = 6.96\lambda$. (a) No window. (b) 64 glassless windows. $a^i = 0.87\lambda$, $b^i = 1.20\lambda$.

building model with the bistatic angle of 45°. Then, the building model is rotated clockwise. The first model simulates a building without windows, while the second model is designed with $64(4 \times 4 \times 4)$ windows. Both building models have the same outer dimensions ($L_x = L_y = 28$ cm (6.09λ), $L_z = 32$ cm (6.96λ)). The model in Fig. 3 (b) has 64 equally aligned glassless windows, each measuring $a^i = 4$ cm (0.87λ) by $b^i = 5.5$ cm (1.20λ).

Figure 5 shows the bistatic scattering patterns of E_ϕ in the horizontal plane ($\theta_0 = \theta = \pi/2$). Measurement data has been adjusted by its peak value. The corresponding results by the PO method from HFSS are also included for the comparison in Fig. 5. Four distinctive main lobes are observed in the specular reflection directions due to the building side walls. These are generated by the building's outer edges. The results derived by the KA method agree well with the results given by the PO method and the measurement results. The

Table 1 Grating angles ϕ_p of building surface $x = L_x/2$ at three different frequencies

f	6.5 GHz	13.0 GHz	30.0 GHz
$p = -2$	286.19°	314.53°	327.76°
$p = -1$	314.53°	326.25°	332.65°
$p = 0$	337.50°	337.50°	337.50°
$p = 1$	0.47°	348.75°	342.35°
$p = 2$	28.81°	0.47°	347.24°

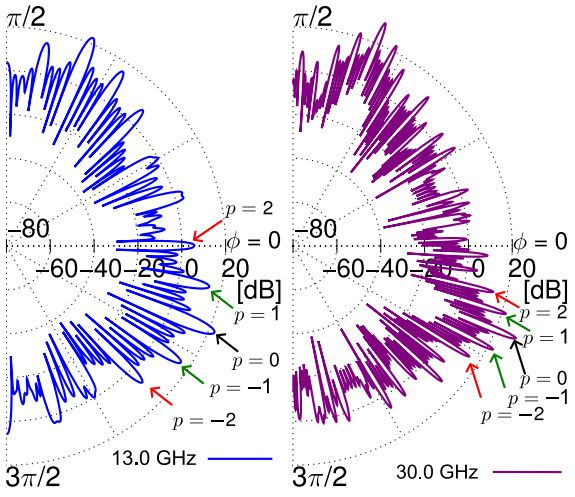

(a) $f = 13.0$ GHz (b) $f = 30.0$ GHz

Fig. 6 The bistatic scattering pattern E_ϕ. All parameters are the same as Fig. 5 (b) except frequency. (a) $f = 13.0$ GHz. (b) $f = 30.0$ GHz.

differences observed in these figures may be attributed to the imperfect fabrication of the two building models, the coupling between the window apertures, and the re-radiations from the internal building structures. When $\theta = \theta_0 = \pi/2$, the roof does not contribute to the overall scattering effect. This is due to the absence of induced surface currents on the roof under these conditions.

For the case of a building with 64 glassless windows in Fig. 5 (b), one observes regular minor lobes due to the periodic window grating effect, in addition to the four main lobes. The observed grating effects can be predicted using the general grating equations (see Appendix B). When these equations are applied to the building wall at $x = L_x/2$, with using a coordinate transformation to account for the differences in the coordinate system, and the condition ($\theta_0 = \theta = \pi/2$), the corresponding equation for the calculation of the grating angles ϕ_p is derived as

$$\phi_p = \arcsin\left(\frac{2\pi p}{kd\sqrt{2+\sqrt{2}}}\right) - \frac{\pi}{8}, \tag{24}$$

where d is the periodic spacing between windows in the y-direction, and p is the corresponding Floquet mode number. It should be noted that the additional Floquet mode number q is not appeared in this case due to $\theta_0 = \theta = \pi/2$. Table 1 presents the grating angles (ϕ_p) for the building wall at $x = L_x/2$ for three different frequencies: 6.5 GHz, 13.0

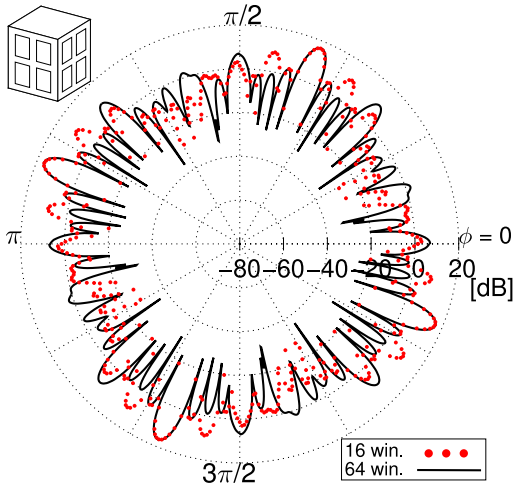

Fig. 7 Comparison of the bistatic scattering pattern E_ϕ between buildings with 16 and 64 glassless windows. All parameters are the same as in Fig. 5 (b), except $a^i = 1.74\lambda$, $b^i = 2.40\lambda$ for the 16 windows building.

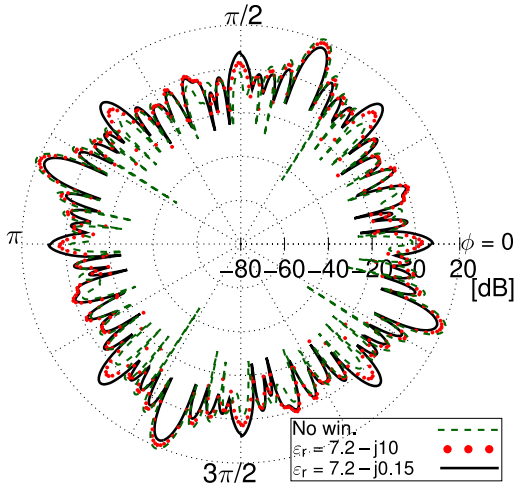

Fig. 9 Comparison of the bistatic scattering pattern E_ϕ among buildings with high-loss glass windows ($\varepsilon_r = 7.2 - j10.0$), with practical glass windows ($\varepsilon_r = 7.2 - j0.15$), and without windows. Other parameters are the same as in Fig. 8.

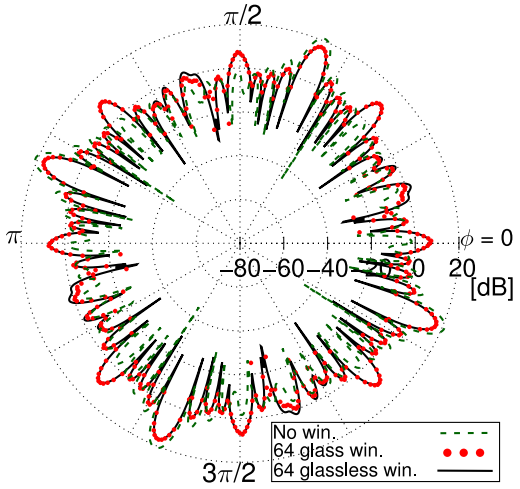

Fig. 8 Comparison of the bistatic scattering pattern E_ϕ among three buildings: no window, 64 windows with/without glass. All parameters are the same as in Fig. 5 (b), except dielectric glasses ($\varepsilon_r = 7.20 - j0.15$) are set at the top of each window ($f^i = 0$). The glass thickness ($g^i - f^i$) is 0.03λ.

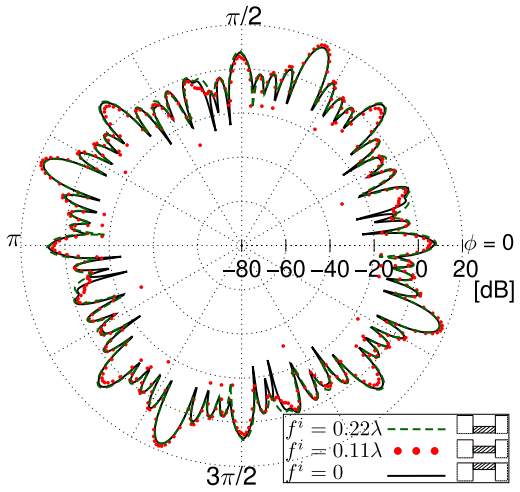

Fig. 10 Comparison of the bistatic scattering pattern E_ϕ among buildings with 64 windows when the location of glass is changed. All parameters are the same as in Fig. 8.

GHz, and 30.0 GHz. The angles are computed for the Floquet mode numbers p ranging from −2 to 2. Scattering fields at 13.0 GHz and 30.0 GHz are shown in Fig. 6 to investigate the frequency dependence of the grating effects. The corresponding zeroth-order grating lobe ($p = 0$) predicts the specular angle of 337.5° regardless of frequency. As the frequency increases, the grating angles for non-zero mode numbers shift toward the specular angle. When comparing the scattering patterns in Figs. 5 (b) and 6, the fields at higher frequencies show stronger, sharper main lobes, along with a greater number of diffraction lobes. One observes that although our building wall has four horizontal windows per row, the corresponding grating lobes may be estimated well by a grating equation of an infinite periodic array of the structures.

It might be interesting to analyze the impact of window size on the scattering far-field. Figure 7 illustrates a comparison of the scattered far-fields for two building models: one with 64 smaller windows and another with 16 double-sized windows. While the four main lobes are the same, the location and the level of minor grating lobes change due to the alignment and size of the windows.

Let us now discuss the effect of the window glass with practical parameters for wireless communication. Figure 8 shows the scattering far-field patterns for three building models: no window, 64 windows with/without glass. The electrical property of the glass is selected as $\varepsilon_r = 7.2 - j0.15$, $\mu_r = 1$ for soda-silica glass [31]. The window glass with the thickness ($g^i - f^i = 0.03\lambda$) is installed on the upper window aperture ($f^i = 0$). In the comparison of the building models with and without windows, the difference at the main lobes

is approximately 4 ∼ 5 dB. The main scattering feature is same for two models with windows. Since the glass is pretty thin ($g^i - f^i < 0.1\lambda$) and its loss is small, the effect on the grating lobes is weak.

In order to observe the effect of the loss of the glass, Fig. 9 shows the pattern changes for different relative dielectric constants $\varepsilon_r[= 7.2 - j0.15, 7.2 - j10.0, 7.2 - j\infty(\text{PEC})]$. One observes that as the loss gets bigger, the periodic window grating lobes become weaker, and the main lobes become stronger. Consequently, a building with highly lossy glass windows exhibits similar scattering characteristics to a building without windows. This evidence also validates our KA formulation to the scattering by buildings with/without window glass.

Finally, Fig. 10 shows the change in the scattering far-field pattern due to the location of the window glass. The far-field patterns by three different positions: $f^i = 0, 0.11\lambda, 0.22\lambda$ are compared here. The differences among the three cases are small but they primarily occur in the grating lobes, which are affected by changes in the modal reflection coefficients as described in Eqs. (12), (13).

4. Conclusion

This paper has presented a high-frequency analysis of plane wave scattering by buildings with multiple windows using the KA method. When the distance between the windows and the building edges is larger than the wavelength, the scattering field can be obtained by summing the radiation from the magnetic currents excited on the virtually closed apertures on the windows and the exterior of the building wall. The magnetic currents are generated by the incident plane wave and the reflected waveguide modal field excited by the window glass interface.

Two scale building models have been constructed and utilized to measure the scattered fields in an anechoic chamber room. Our results are in good agreement with these measurement results and the one obtained by the PO method. The effects of the glass, window aperture dimensions have also been discussed. While the main beams are mostly dependent on the edges of the building, the grating minor lobes depend on the location of the multiple windows.

The difference between the measured data and our analytical result may suggest the manufacturing precision of the models, the effect of coupling between the windows and the internal field re-radiated to the outside of the building. All these aspects are currently under investigation. Future work will also consider the polarization difference to enhance the KA accuracy and provide a more comprehensive understanding of urban radio communication.

Acknowledgments

A part of this work has been supported by a Scientific Research Grant In Aide (23K03860, 2023) from the Japan Society for the Promotion of Science, Japan, and 2023 Chuo University Personal Research Grant.

References

[1] L.H. Bertoni, Radio Propagation for Modern Wireless Systems, Prentice-Hall, New Jersey, 2000.
[2] P.M. Morse and P.J. Rubenstein, "The diffraction of waves by ribbons and by slits," Phys. Rev., vol. 54, no. 11, pp. 895–898, Dec. 1938. DOI: 10.1103/PhysRev.54.895
[3] S. Kashyap and M.A.K. Hamid, "Diffraction characteristics of a slit in a thick conducting screen," IEEE Trans. Antennas and Propag., vol. 19, no. 4, pp. 499–507, July 1971. DOI: 10.1109/TAP.1971.1139961
[4] S.H. Kang, H.J. Eom, and T.J. Park, "TM scattering from a slit in a thick conducting screen: Revisited," IEEE Trans. Microw. Theory Techn., vol. 41, no. 5, pp. 895–899, May 1993. DOI: 10.1109/22.234533
[5] T.J. Park, S.H. Kang, and H.J. Eom, "TE scattering from a slit in a thick conducting screen: Revisited," IEEE Trans. Antennas and Propag., vol. 42, no. 1, pp. 112–114, Jan. 1994. DOI: 10.1109/8.272309
[6] J.M. Jin and J.L. Volakis, "TE scattering by an inhomogeneously filled aperture in a thick conducting plane," IEEE Trans. Antennas and Propag., vol. 38, no. 8, pp. 1280–1286, Aug. 1990. DOI: 10.1109/8.56967
[7] J.M. Jin and J.L. Volakis, "Electromagnetic scattering by and transmission through a three-dimensional slot in a thick conducting plane," IEEE Trans. Antennas and Propag., vol. 39, no. 4, pp. 543–550, Apr. 1991. DOI: 10.1109/8.81469
[8] Y. Nomura and S. Katsura, "Diffraction of electromagnetic waves by ribbon and slit. I," J. Phys. Soc. Jpn., vol. 12, no. 2, pp. 190–200, 1957. DOI: 10.1143/JPSJ.12.190
[9] K. Hongo and G. Ishii, "Diffraction of an electromagnetic plane wave by a thick slit," IEEE Trans. Antennas Propag., vol. 26, no. 3, pp. 494–499, May 1978. DOI: 10.1109/TAP.1978.1141870
[10] H. Serizawa, "Diffraction by a rectangular hole in a thick conducting screen," Novel Imaging and Spectroscopy. IntechOpen, 2019. DOI: 10.5772/intechopen.89029
[11] M. Ando, "Physical optics," in Analysis Methods for Electromagnetic Wave Problems, Chap. 4, ed. E. Yamashita, Artech House, Boston, USA, 1990.
[12] L. Diaz and T. Milligam, Antenna Engineering Using Physical Optics, Artech House, Norwood, MA, USA, 1996.
[13] H.N. Quang and H. Shirai, "A new interpretation of physical optics approximation from surface equivalence theorem," IEICE Trans. on Electron., vol. E101-C, no. 8, pp. 664–670, Aug. 2018. DOI: 10.1587/transele.E101.C.664
[14] H.N. Quang and H. Shirai, "High frequency electromagnetic scattering analysis by rectangular cylinders –TM polarization–," IEICE Trans. on Electron., vol. E102-C, no. 1, pp. 21–29, Jan. 2019. DOI: 10.1587/transele.E102.C.21
[15] J.B. Keller, "Diffraction by an aperture," J. Appl. Phys., vol. 28, pp. 426–444, 1957. DOI: 10.1063/1.1722767
[16] J.B. Keller, "Geometrical theory of diffraction," J. Opt. Soc. Am., vol. 52, no. 2, pp. 116–130, 1962. DOI: 10.1364/JOSA.52.000116
[17] G.L. James, Geometrical Theory of Diffraction for Electromagnetic Waves, Peter Peregrinus Ltd, 1976.
[18] R.C. Hansen, ed., Geometrical Theory of Diffraction, IEEE Press, New Jersey, 1981.
[19] H. Shirai, Geometrical Theory of Diffraction, Corona Publ. Co., Japan, 2015 (in Japanese).
[20] H. Shirai, M. Shimizu and R. Sato, "Hybrid ray-mode analysis of E-polarized plane wave diffraction by a thick slit," IEEE Trans. Antennas and Propag., vol. 64, no. 11, pp. 4828–4835, Nov. 2016. DOI: 10.1109/TAP.2016.2608978
[21] M. Shimizu, H. Shirai and R. Sato, "Electromagnetic scattering analysis by a window model on a building wall," IEICE Trans. Electron., vol. J100-C, no. 7, pp. 295–301, July 2017 (in Japanese).

[22] P. Pongsilamanee and H.L. Bertoni, "Specular and nonspecular scattering from building facades," IEEE Trans. Antennas and Propag., vol. 52, no. 7, pp. 1879–1889, July 2004. DOI: 10.1109/TAP.2004.831317

[23] S. Kwon, I.S. Koh, H.W. Moon, J.W. Lim and Y.J. Yoon, "Model of inhomogeneous building facade for ray tracing method," Electron. Lett., vol. 44, no. 23, pp. 1341–1342, Nov. 2008. DOI: 10.1049/el:20081651

[24] L.B. Felsen and H. Shirai, "Hybrid ray-mode analysis of high-frequency wave coupling into large waveguides and cavities," Optics Lett., vol. 12, no. 1, pp. 7–9, 1987. DOI: 10.1364/OL.12.000007

[25] H. Shirai and L.B. Felsen, "Rays, modes and beams for plane wave coupling into a wide open-ended parallel-plane waveguide," Wave Motion, vol. 9, no. 4, pp. 301–317, July 1987. DOI: 10.1016/0165-2125(87)90003-5

[26] H. Shirai and L.B. Felsen, "Rays and modes for plane wave coupling into a large open-ended circular waveguide," Wave Motion, vol. 9, no. 6, pp. 461–482, Nov. 1987. DOI: 10.1016/0165-2125(87)90016-3

[27] K.N. Nguyen and H. Shirai, "Kirchhoff approximation analysis of plane wave scattering by conducting thick slits," IEICE Trans. on Electron., vol. E102-C, no. 1, pp. 12–20, Jan. 2019. DOI: 10.1587/transele.E102.C.12

[28] K.N. Nguyen, H. Shirai and H. Serizawa, "Electromagnetic scattering analysis from a rectangular hole in a thick conducting screen," IEICE Trans. Electron., vol. E104-C, no. 4, pp. 134–143, 2021. DOI: 10.1587/transele.2020REP0001

[29] C.M. Bui, K.N. Nguyen and H. Shirai, "Electromagnetic wave scattering analysis by a window aperture on a conducting wall," Progress In Electromagnetics Research C, vol. 122, pp. 95–108, 2022. DOI: 10.2528/PIERC22041501

[30] C.A. Balanis, Advanced Engineering Electromagnetics, 2nd ed., Wiley, New Jersey, 2012.

[31] A.R.V. Hippel, Dielectric Materials and Applications, MIT Press, New York, 1954.

[32] A.K. Bhattacharyya, Phased Array Antennas: Floquet Analysis, Synthesis, BFNs, and Active Array Systems, Wiley, New Jersey, 2006.

Appendix A: Scattering fields by other walls

A.1 Scattering fields by building wall at $y = L_y/2$

One might derive the scattering field $\boldsymbol{E}^{(3)}$ by the outer edges of the building wall at $y = L_y/2$ as:

$$E_r^{(3)} \sim E_\theta^{(3)} \sim 0, \tag{A·1}$$

$$\begin{aligned} E_\phi^{(3)} \sim{}& \mathrm{U}(\pi-\phi_0)\,\mathrm{sgn}(\phi-\pi) \\ &\cdot \frac{jA_\phi e^{-jkr}}{2\pi kr} k^2 L_x L_z e^{-j\gamma k L_z/2} e^{j\beta k L_y/2} \\ &\cdot \mathrm{sinc}\left(\frac{\gamma k L_z}{2}\right) \mathrm{sinc}\left(\frac{\alpha k L_x}{2}\right) \sin\theta \sin\phi_0. \end{aligned} \tag{A·2}$$

The scattering field $\overline{\boldsymbol{E}}^{(3)}$ by N windows ($d_y^i = L_y/2$) is presented as

$$\overline{E}_r^{(3)} \sim 0, \tag{A·3}$$

$$\begin{aligned} \overline{E}_\theta^{(3)} \sim{}& -\mathrm{U}(\pi-\phi_0)\,\mathrm{U}(\pi-\phi) \\ &\cdot \frac{jA_\phi e^{-jkr}}{2\pi kr} \sum_{i=1}^{N} e^{jk[\alpha d_x^i + \beta(L_y/2) + \gamma d_z^i]} \\ &\cdot \sum_{m=0}^{\infty}\sum_{n=0}^{\infty} \frac{(k^2 a^i b^i)^2 B_{m,n}^{(3)} \cos\theta \sin\phi}{(m\pi/ka^i)^2 + (n\pi/kb^i)^2} \\ &\cdot \left\{ \left(\frac{m\pi}{ka^i}\right)^2 R_{m,n} M_{m,n}^{(3)} - \frac{mn\pi^2}{k^2 a^i b^i} \overline{R}_{m,n} N_{m,n}^{(3)} \right\}, \end{aligned} \tag{A·4}$$

$$\begin{aligned} \overline{E}_\phi^{(3)} \sim{}& \mathrm{U}(\pi-\phi_0)\,\mathrm{U}(\pi-\phi) \\ &\cdot \frac{jA_\phi e^{-jkr}}{2\pi kr} \sum_{i=1}^{N} e^{jk[\alpha d_x^i + \beta(L_y/2) + \gamma d_z^i]} \\ &\cdot \left\{ k^2 a^i b^i\, \mathrm{sinc}\left(\frac{ka^i\alpha}{2}\right) \mathrm{sinc}\left(\frac{kb^i\gamma}{2}\right) \sin\theta \sin\phi_0 \right. \\ &- \sum_{m=0}^{\infty}\sum_{n=0}^{\infty} \frac{(k^2 a^i b^i)^2 B_{m,n}^{(3)} \cos\phi}{(m\pi/ka^i)^2 + (n\pi/kb^i)^2} \\ &\cdot \left\{ R_{m,n} M_{m,n}^{(3)} \left[\left(\frac{m\pi}{ka^i}\right)^2 \cos^2\theta - \left(\frac{n\pi}{kb^i}\right)^2 \sin^2\theta \right] \right. \\ &\left. \left. - \frac{mn\pi^2}{k^2 a^i b^i} \overline{R}_{m,n} N_{m,n}^{(3)} \right\} \right\}, \end{aligned} \tag{A·5}$$

where

$$\begin{aligned} B_{m,n}^{(3)} = {}& \frac{(-1)^{m+1} e^{j(ka^i/2)\sin\theta\cos\phi} + e^{-j(ka^i/2)\sin\theta\cos\phi}}{(m\pi)^2 - (ka^i \sin\theta\cos\phi)^2} \\ &\cdot \frac{(-1)^{n+1} e^{j(kb^i/2)\cos\theta} + e^{-j(kb^i/2)\cos\theta}}{(n\pi)^2 - (kb^i\cos\theta)^2}, \end{aligned} \tag{A·6}$$

$$M_{m,n}^{(3)} = -\frac{n^2\pi^2 \epsilon_m \epsilon_n a^i}{2b^i} \sin\theta_0 \sin(2\phi_0) \overline{B}_{m,n}^{(3)}, \tag{A·7}$$

$$N_{m,n}^{(3)} = 2mn\pi^2 \sin\theta_0 \sin(2\phi_0) \overline{B}_{m,n}^{(3)}, \tag{A·8}$$

$$\begin{aligned} \overline{B}_{m,n}^{(3)} = {}& \frac{(-1)^{m+1} e^{j(ka^i/2)\sin\theta_0\cos\phi_0} + e^{-j(ka^i/2)\sin\theta_0\cos\phi_0}}{(m\pi)^2 - (ka^i \sin\theta_0\cos\phi_0)^2} \\ &\cdot \frac{(-1)^{n+1} e^{j(kb^i/2)\cos\theta_0} + e^{-j(kb^i/2)\cos\theta_0}}{(n\pi)^2 - (kb^i\cos\theta_0)^2}. \end{aligned} \tag{A·9}$$

A.2 Scattering fields by building wall at $x = -L_x/2$

One might derive the scattering field $\boldsymbol{E}^{(4)}$ by the outer edges of the building wall at $x = -L_x/2$ as:

$$E_r^{(4)} \sim E_\theta^{(4)} \sim 0, \tag{A·10}$$

$$\begin{aligned} E_\phi^{(4)} \sim{}& \mathrm{U}\left(\phi_0 - \frac{\pi}{2}\right) \mathrm{U}\left(\frac{3\pi}{2} - \phi_0\right) \mathrm{sgn}\left(\phi - \frac{\pi}{2}\right) \mathrm{sgn}\left(\frac{3\pi}{2} - \phi\right) \\ &\cdot \frac{jA_\phi e^{-jkr}}{2\pi kr} k^2 L_y L_z e^{-j\gamma k L_z/2} e^{-j\alpha k L_x/2} \\ &\cdot \mathrm{sinc}\left(\frac{\gamma k L_z}{2}\right) \mathrm{sinc}\left(\frac{\beta k L_y}{2}\right) \sin\theta \cos\phi_0. \end{aligned} \tag{A·11}$$

The scattering field $\overline{\boldsymbol{E}}^{(4)}$ by N windows ($d_x^i = -L_x/2$) is presented as

$$\overline{E}_r^{(4)} \sim 0, \tag{A·12}$$

$$\overline{E}_\theta^{(4)} \sim -\mathrm{U}\left(\phi_0 - \frac{\pi}{2}\right) \mathrm{U}\left(\frac{3\pi}{2} - \phi_0\right) \mathrm{U}\left(\phi - \frac{\pi}{2}\right) \mathrm{U}\left(\frac{3\pi}{2} - \phi\right)$$

$$\cdot \frac{jA_\phi e^{-jkr}}{2\pi kr} \sum_{i=1}^{N} e^{jk[-\alpha(L_x/2)+\beta d_y^i+\gamma d_z^i]}$$
$$\cdot \sum_{m=0}^{\infty}\sum_{n=0}^{\infty} \frac{(k^2a^ib^i)^2 B_{m,n}^{(2)} \cos\theta\cos\phi}{(m\pi/ka^i)^2+(n\pi/kb^i)^2}$$
$$\cdot \left[\left(\frac{m\pi}{ka^i}\right)^2 R_{m,n} M_{m,n}^{(2)} + \frac{mn\pi^2}{k^2a^ib^i}\overline{R}_{m,n} N_{m,n}^{(2)}\right], \quad (A\cdot 13)$$

$$\overline{E}_\phi^{(4)} \sim -\mathrm{U}\left(\phi_0-\frac{\pi}{2}\right)\mathrm{U}\left(\frac{3\pi}{2}-\phi_0\right)\mathrm{U}\left(\phi-\frac{\pi}{2}\right)\mathrm{U}\left(\frac{3\pi}{2}-\phi\right)$$
$$\cdot \frac{jA_\phi e^{-jkr}}{2\pi kr} \sum_{i=1}^{N} e^{jk[-\alpha(L_x/2)+\beta d_y^i+\gamma d_z^i]}$$
$$\cdot \left\{ k^2a^ib^i \,\mathrm{sinc}\left(\frac{ka^i\beta}{2}\right)\mathrm{sinc}\left(\frac{kb^i\gamma}{2}\right)\cos\phi_0\sin\theta \right.$$
$$+ \sum_{m=0}^{\infty}\sum_{n=0}^{\infty} \frac{(k^2a^ib^i)^2 B_{m,n}^{(2)} \sin\phi}{(m\pi/ka^i)^2+(n\pi/kb^i)^2}$$
$$\cdot \left\{ R_{m,n} M_{m,n}^{(2)} \left[\left(\frac{n\pi}{kb^i}\right)^2 \sin^2\theta - \left(\frac{m\pi}{ka^i}\right)^2 \cos^2\theta\right] \right.$$
$$\left.\left. - \frac{mn\pi^2}{k^2a^ib^i}\overline{R}_{m,n} N_{m,n}^{(2)} \right\}\right\}. \quad (A\cdot 14)$$

A.3 Scattering fields by building wall at $y = -L_y/2$

One might derive the scattering field $\boldsymbol{E}^{(5)}$ by the outer edges of the building wall at $y = -L_y/2$ as:

$$E_r^{(5)} \sim E_\theta^{(5)} \sim 0, \quad (A\cdot 15)$$
$$E_\phi^{(5)} \sim \mathrm{U}(\phi_0-\pi)\,\mathrm{sgn}(\phi-\pi)$$
$$\cdot \frac{jA_\phi e^{-jkr}}{2\pi kr} k^2 L_x L_z e^{-j\gamma kL_z/2} e^{-j\beta kL_y/2}$$
$$\cdot \mathrm{sinc}\left(\frac{\gamma kL_z}{2}\right)\mathrm{sinc}\left(\frac{\alpha kL_x}{2}\right)\sin\theta\sin\phi_0. \quad (A\cdot 16)$$

The scattering field $\overline{\boldsymbol{E}}^{(5)}$ by N windows ($d_y^i = -L_y/2$) is presented as

$$\overline{E}_r^{(5)} \sim 0, \quad (A\cdot 17)$$
$$\overline{E}_\theta^{(5)} \sim \mathrm{U}(\phi_0-\pi)\,\mathrm{U}(\phi-\pi)$$
$$\cdot \frac{jA_\phi e^{-jkr}}{2\pi kr} \sum_{i=1}^{N} e^{jk[\alpha d_x^i-\beta(L_y/2)+\gamma d_z^i]}$$
$$\cdot \sum_{m=0}^{\infty}\sum_{n=0}^{\infty} \frac{(k^2a^ib^i)^2 B_{m,n}^{(3)} \cos\theta\sin\phi}{(m\pi/ka^i)^2+(n\pi/kb^i)^2}$$
$$\cdot \left\{\left(\frac{m\pi}{ka^i}\right)^2 R_{m,n} M_{m,n}^{(3)} - \frac{mn\pi^2}{k^2a^ib^i}\overline{R}_{m,n} N_{m,n}^{(3)}\right\}, \quad (A\cdot 18)$$
$$\overline{E}_\phi^{(5)} \sim -\mathrm{U}(\phi_0-\pi)\,\mathrm{U}(\phi-\pi)$$
$$\cdot \frac{jA_\phi e^{-jkr}}{2\pi kr} \sum_{i=1}^{N} e^{jk[\alpha d_x^i-\beta(L_y/2)+\gamma d_z^i]}$$

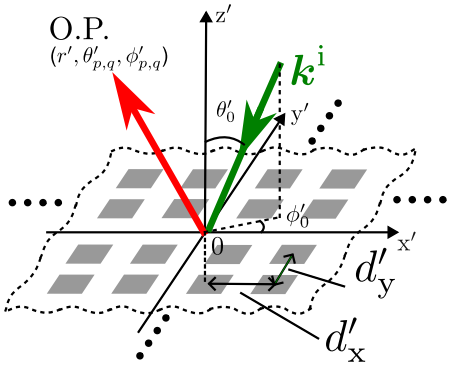

Fig. A·1 The 2D periodic array on the x′-y′ plane at $z' = 0$.

$$\cdot \left\{ k^2a^ib^i \,\mathrm{sinc}\left(\frac{ka^i\alpha}{2}\right)\mathrm{sinc}\left(\frac{kb^i\gamma}{2}\right)\sin\theta\sin\phi_0 \right.$$
$$- \sum_{m=0}^{\infty}\sum_{n=0}^{\infty} \frac{(k^2a^ib^i)^2 B_{m,n}^{(3)} \cos\phi}{(m\pi/ka^i)^2+(n\pi/kb^i)^2}$$
$$\cdot \left\{ R_{m,n} M_{m,n}^{(3)} \left[\left(\frac{m\pi}{ka^i}\right)^2 \cos^2\theta - \left(\frac{n\pi}{kb^i}\right)^2 \sin^2\theta\right] \right.$$
$$\left.\left. - \frac{mn\pi^2}{k^2a^ib^i}\overline{R}_{m,n} N_{m,n}^{(3)} \right\}\right\}. \quad (A\cdot 19)$$

Appendix B: Grating equations

As shown in Fig. A·1, a plane wave with a wave vector $\boldsymbol{k}^i$ is obliquely incident (θ'_0, ϕ'_0) on an infinite periodic structure with the periods d'_x and d'_y in the x′ and y′ directions, respectively. According to Floquet's theorem [32], the scattering field $\boldsymbol{E}^s$ can then be represented as

$$\boldsymbol{E}^s(x', y', z') = \sum_{p=-\infty}^{\infty}\sum_{q=-\infty}^{\infty} \boldsymbol{E}_{p,q}^s(z') e^{-j(-k\sin\theta'_0\cos\phi'_0+2\pi p/d'_x)x'}$$
$$\cdot e^{-j(-k\sin\theta'_0\sin\phi'_0+2\pi q/d'_y)y'}, \quad (A\cdot 20)$$

where $\boldsymbol{E}_{p,q}^s(z')$ denotes the vector function that describes the field variations along the z′-direction, and depends on the specific structure of the periodic array and the incident wave. The integers p, q are the Floquet mode numbers with respect to the x′ and y′ directions. Moreover, the scattered field $\boldsymbol{E}^s$ can be presented by an infinite sum of Floquet space harmonics as

$$\boldsymbol{E}^s(x', y', z') = \sum_{p=-\infty}^{\infty}\sum_{q=-\infty}^{\infty} \boldsymbol{E}_{p,q}^s(z') e^{-jkx'\sin\theta'_{p,q}\cos\phi'_{p,q}}$$
$$\cdot e^{-jky'\sin\theta'_{p,q}\sin\phi'_{p,q}}. \quad (A\cdot 21)$$

Comparing Eqs. (A·20) and (A·21), the grating equations for the scattering angles $\theta'_{p,q}, \phi'_{p,q}$ can be given as

$$\sin\theta'_{p,q}\cos\phi'_{p,q} + \sin\theta'_0\cos\phi'_0 = \frac{2\pi p}{kd'_x}, \quad (A\cdot 22)$$
$$\sin\theta'_{p,q}\sin\phi'_{p,q} + \sin\theta'_0\sin\phi'_0 = \frac{2\pi q}{kd'_y}. \quad (A\cdot 23)$$

Cuong Manh Bui received the B.E. and the M.S. degrees in Telecommunication Engineering from Hanoi University of Science and Technology in 2017 and 2020, respectively. He is now a Ph.D. student at Chuo University. His current research interest is electromagnetic scattering. Mr. Bui is a student member of the IEEE.

Hiroshi Shirai received the B.E. and the M.E. degrees in Electrical Engineering from Shizuoka University, Japan, in 1980 and 1982, respectively, and the Ph.D. degree from Polytechnic University (presently renamed as Tandon School of Engineering, New York University), New York in 1986. He was a Research Fellow, then a Postdoctoral Scientist until March 1987 at Polytechnic University. Since April 1987, he has been with Chuo University, Tokyo, Japan, where he is currently a Professor. He has been serving as a committee member of various technical societies and international meetings. He is now an Editorial Advisory member of IEICE Fundamentals Review. He received the R.W.P. King Best Paper Award from the Antennas and Propagation Society of the IEEE in 1987, the IEICE Electronics Society Award in 2019, and the IEICE Best Paper Award in 2020. His current research interests include wave propagation and diffraction in time harmonic and transient domains. Dr. Shirai is a Fellow of the Electromagnetic Academy, a life senior member of the IEEE, a member of Sigma Xi, and the IEE of Japan.